Steel and Composite Structures, *Vol. 26, No. 1 (2018) 31-44*
DOI: https://doi.org/10.12989/scs.2018.26.1.031

Mechanical performance of a new I-section weak-axis column bending connection

Linfeng Lu[*1], Yinglu Xu[1a] and James B.P. Lim[2b]

[1]*School of Civil Engineering, Chang'an University, 75 Chang'an Middle Rd, Xi'an, PR China*
[2]*Department of Civil and Environmental Engineering, University of Auckland (City Campus), Engineering Building, 20 Symonds Street, Auckland, New Zealand*

(*Received July 24, 2017, Revised September 15, 2017, Accepted September 23, 2017*)

Abstract. This paper reports a novel steel beam-to-column connection suitable for use in the weak axis of I-section column. Monotonic and cyclic loading experimental investigations and numerical analysis of the proposed weak-axis connection were conducted, and the calculation procedure of the beam-column relative rotation angle and plastic rotation angle was developed and described in details. A comparative analysis of mechanical property and steel consumption were employed for the proposed I-section column weak-axis connection and box-section column bending connection. The result showed that no signs of fracturing were observed and the plastic hinge formed reliably in the beam section away from the skin plate under the beam end monotonic loading, and the plastic hinge formed much closer to the skin plate under the beam end cyclic loading. The fracture of welds between diaphragm and skin plate would cause an unstable hysteretic response under the column top horizontal cyclic loading. The proposed weak-axis connection system could not only simplify the design calculation progress when I-section column is adopted in frame structural design but also effectively satisfy the requirements of 'strong joint and weak member', as well as lower steel consumption.

Keywords: steel frame; weak-axis; bending connection; panel zone; I-section column; constructability

1. Introduction

During the 1994 Northridge and 1995 Kobe earthquakes, extensive welded-flange-bolted-web beam-to-column connections suffered unexpected brittle fractures, which has raised concerns regarding the reliability of the Pre-Northridge connection method and prompted engineers to rethink the design of connections and construction details of connections in steel moment frames. Extensive work has been conducted to find methods to improve the seismic performance of steel moment connections, and a wide variety of solutions have been proposed during the past decades, many of which have shown satisfactory levels of cyclic performance in the laboratory or numerical analysis. However, all the various types of connections based on two concepts of (i) strengthening the connection; and (ii) weakening the beam ends. The overall goal in the development of new connections is to provide a highly ductile response, reliable performance, and also the economy. Based on the post-Northridge connection research, the beam-to-column connections for special moment frames shall be capable of accommodating a minimum plastic rotation capacity of 0.03 rad (FEMA-267 1995), or a story drift angle of at least 0.04 rad (ANSI/AISC 341-10 2010) while the measured flexural resistance of the connection at the face of column shall equal at least 0.80 times the nominal plastic flexural strength M_p of the beam. Substantially all the previous researches dealt with steel moment connections for the strong-axis bending connection. For the weak-axis connections, limited research has been done so far. The pertinent study concerning weak-axis moment connections to my knowledge, especially some new types of weak-axis connections, were performed by several researchers.

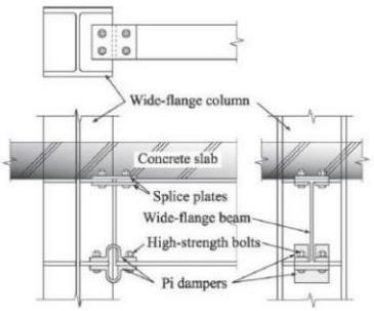

Fig. 1 Connection of Koetaka

Koetaka *et al*. (2005) proposed a novel weak-axis column bending connection with hysteretic dampers (Fig. 1). Their test demonstrated that the proposed connection was able to achieve stable hysteretic performance in a large deformation range because yielding was limited only in the dampers. Cabrero and Bayo (2007a, b) performed an

∗Corresponding author, Professor
E-mail: lulinfeng@chd.edu.cn
[a]Ph.D. Student
E-mail: 2015028003@chd.edu.cn
[b]Associate Professor
E-mail: james.lim@auckland.ac.nz

ISSN: 1229-9367 (Print), 1598-6233 (Online)

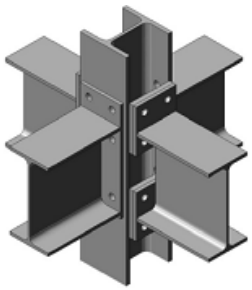

Fig. 2 Connection of Cabrero

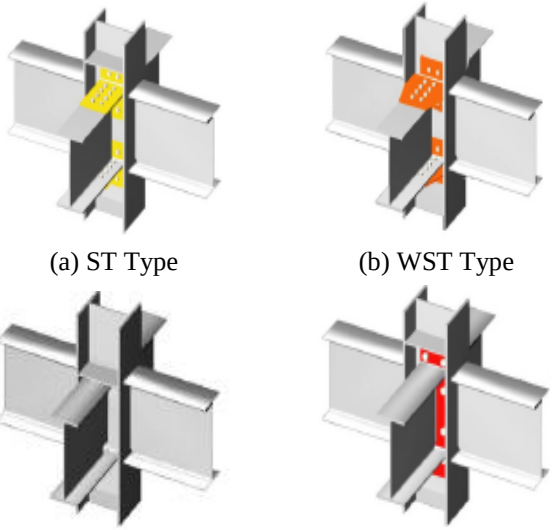

(a) ST Type (b) WST Type

(c) EP Type (d) BA Type

Fig. 3 Connection forms of Kim

experimental and a theoretical study to investigate the behavior of extended end-plate connections in both major and minor column axis subjected to a three-dimensional loading (Fig. 2). And the tested minor-axis joints consisted of two partial end-plates outside welded to the of column flange. Similarly, Kim *et al*. (2008) proposed three new types of weak axis connection details with welded split plates and end plates (Fig. 3). They reported that these types were easy-to-construct and also ensure the flexural behavior of weak-axis moment connections. This kind of weak axis connection was tested and reported again by Lee *et al*. (2016), Lee *et al*. (2013, 2014), and they investigated the seismic performance of six types of weak-axis column-tree connections through cyclic testing for six full-scale specimens. The effects of beam splice length on the seismic performance of weak-axis column-tree connections were experimentally investigated. Additional work has been conducted by Shim *et al*. (2014), and they proposed a weak-axis system, which mainly used bolts (Fig. 4). In their research, eight interior joint specimens were tested to verify the structural behavior of the proposed connection, and their test results demonstrated that it behaved better than the standard weak-axis connection and had excellent constructability. Kozlowski (2016) presented a comprehensive analytical model to predict the moment resistance, initial stiffness, and rotation capacity of the semi-rigid weak axis composite connections and a

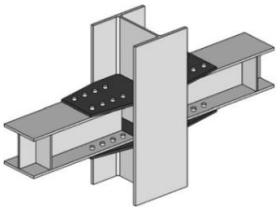

Fig. 4 Connection of Shim

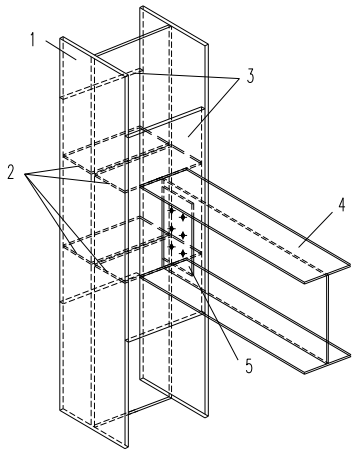

1- I-shaped column
2- Diaphragm
3- Skin plate
4- I-shaped beam
5- Shear plate

Fig. 5 Weak-axis column bending connection with box-strengthened panel zone

comparative analysis with test results showed a good correlation.

The above previous research, conducted mainly on semi-rigid weak-axis connections, while a few studies have been done on the weak-axis rigid connections which are most commonly used in the practical project in the world. Hence, this paper proposed a novel weak-axis column bending connection with box-strengthened panel zone to make the weak-axis connection much like that of strong-axis, as shown in Fig. 5. The panel zone means the column web region enclosed by column flanges and diaphragms in the strong-axis of I-section column, and similarly, in the proposed weak-axis connection, the panel zone means the column flange region enclosed by skin plates and diaphragms. This paper is organized as follows. Section 2 introduces the construction procedure of the developed weak-axis connection specifics. Section 3 and Section 4 reports the monotonic and cyclic loading test of the proposed connection respectively, and also the corresponding numerical analysis is presented. Successively, the influence of using the proposed connection into a steel frame on the mechanical property is discussed in Section 5. With the connection shown in Fig. 5 as a standard prototype, a series of weak-axis connection forms can be obtained, which are displayed in section 6. Finally, conclusions are drawn in Section 7.

2. Construction procedure of the developed weak-axis connection

The configuration of the developed weak-axis connection specifics was shown in Fig. 5. The main feature

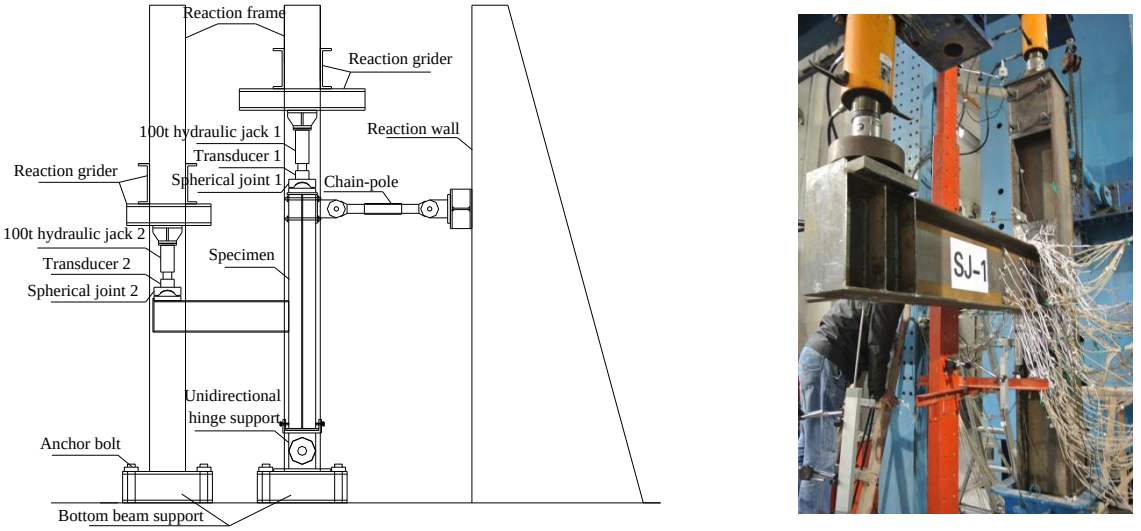

(a) Testing apparatus diagram (b) Specimen installation

Fig. 6 Test setup of monotonic loading

of the proposed weak-axis connection is the closed panel zone formed by the column flanges, column web, diaphragms and skin plates, making the connection in weak-axis as convenient as in the strong-axis. This developed weak-axis connection can be constructed by the following procedure: (1) Cut the steel plates for transverse stiffeners with the thickness equal to or slightly greater than the beam flange, and weld them to the column aligned with the beam flange position. (2) Weld two skin plates between the tips of two column flanges, and weld the stiffeners to the skin plates, to form a box-strengthened panel zone. (3) Apply double-sided fillet welding to weld the shear plate and skin plate. In practice, all the welding up to this step can be performed in the factory to ensure its quality. (4) Use high-strength bolts to connect beam and column temporarily. (5) Utilize complete joint penetration (CJP) groove welds to weld the beam flanges to the skin plate. Last, tighten the frictional high-strength bolts using the calibrated wrench method.

Hence, the proposed weak-axis connection, not only simple to manufacture but also easy to construct, can enable the weak-axis column bending connection to perform like that of strong-axis. The skin plates act as vertical stiffeners for the weak-axis and contribute to the resistance of shear deformation as the closed box panel zone increases the volume of panel zone, and also contribute to the force flow towards the column flanges.

3. Experimental and numerical analysis on an exterior frame joint under monotonic loading

In order to investigate the seismic behavior of the proposed weak-axis connection details, an exterior frame joint was firstly constructed under the assumption that the moment inflection points are close to the mid-height and mid-span of columns and beams respectively. The test setup is shown in Fig. 6. The load was applied vertically at the beam end, with the top and bottom of the column being in connections, and a vertical hydraulic jack was used to apply an axial compression ratio of 0.3 on the top of the column to simulate the effect of the upper floors in a multi-story building.

In general, the behavior of beam-to-column connection has a significant effect on the overall structural response, which is represented by the moment-rotation angle response. While some procedures for calculating the joint rotation angle have been proposed by many researchers, different assumptions were adopted by different researchers, so there is no unified method of joint rotation angle calculation. Hence, a detailed calculation method of the relative ration angle θ of beam and column and also the plastic rotation angle θ_p was presented first as follows.

3.1 Determination of the relative rotation θ of beam and column

Based on the bending moment versus rotation angle relationships, it is readily feasible to characterize and compare the substructure responses in terms of stiffness, strength, and ductility. The bending moments discussed here are computed for $M = Pl$, where P is the reaction force at the beam end, takes the distance l_1 from the loading point to the surface of the skin plate for plotting M-θ hysteretic curves, and l takes the distance L_{CL} between beam span center line and the column axis for plotting M-θ_p hysteretic curves.

While the relative rotation angle of beam and column, θ, is much more difficult to determine accurately, although it has been used very commonly. The rotation contributed to the column and panel zone has always been ignored by most of the yielding and inelastic rotation occurred in the beam. However, the story drift can be definitely separated into three components: the column component, the beam component, and the panel zone component (Lee and Lu 1989). Therefore, in order to better understand the structural behavior, this paper proposed a calculation procedure of the relative rotation angle, which examined the above three

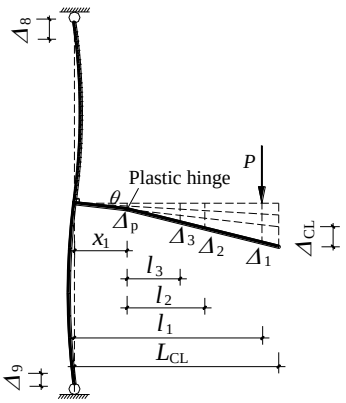

Fig. 7 Calculation diagram of the rotation

components systematically.

The proposed calculation procedure based on the following assumptions: (1) The other parts of the beam are in the elastic state except for the plastic hinge; (2) The axis of the elastic deformation of beam keeps straight after the appearance of the plastic hinge. Under the above two assumptions, when the beam end of exterior frame joint bears concentrated load, the absolute deflection at the beam end includes three parts: the displacement δ_b caused by the elastic deformation of beam, the displacement δ_c caused by the rotation of column (the influence of axial deformation of column was deducted from the beam end absolute displacement) and the displacement θ caused by the relative rotation of beam and column.

3.1.1 Determination of δ_b

Under the concentrated load at the end of a cantilever beam, the elastic deformation of the beam includes elastic bending deformation and elastic shear deformation.

(1)Elastic bending deformation δ_{bb}

According to the basic method of material mechanics, the displacement δ_{bb} of any point of the beam caused by the elastic bending deformation can be calculated as follows.

$$\delta_{\mathrm{bb}} = \int_0^x \frac{\overline{M} M_{\mathrm{P}}}{EI} ds = \frac{Px^2}{6EI}\left(-x + 3l_1\right) \tag{1}$$

where P is the reaction force of loading point at the beam end, E is Young's modulus of steel material, I is sectional inertia moment of the beam, x is the horizontal distance from the surface of the skin plate to any cross section of the beam, and l_1 is the distance between the loading point and the surface of the skin plate.

(2)Elastic shear deformation δ_{bs}

The displacement δ_{bs} of any point of the beam caused by the elastic shear deformation can be calculated as

$$\delta_{\mathrm{bs}} = k\int_0^x \frac{\overline{F}_{\mathrm{Q}} F_{\mathrm{QP}}}{GA} ds = \frac{kPx}{GA} \tag{2}$$

where G is the shear modulus of steel material, A is the sectional area of the beam, and k is a parameter about the section. For I-shaped section, the value of k approximates A/A_1, where A_1 is the area of beam web.

Hence, the elastic deformation δ_b at any point of the beam is calculated as

$$\delta_{\mathrm{b}} = \delta_{\mathrm{bb}} + \delta_{\mathrm{bs}} \tag{3}$$

3.1.2 Determination of δ_c

The box-strengthened panel zone has stronger stiffness than the other part of the I-section column and it remains intact during the tests, as reported by Lu *et al*. (2016a). Hence it is reasonable to regard the column section connected to the skin plates within h distance as elastic. Then the deformation at any point of the beam caused by the rotation of the column can be calculated as

$$\delta_{\mathrm{c}} = \frac{\left|\Delta_4 - \Delta_5\right| \cdot x}{h} \tag{4}$$

where Δ_4 and Δ_5 are the displacement readings from the displacement transducers fixed at upper and lower part of the skin plate respectively, and h is the vertical distance between two displacement transducers.

3.1.3 Determination of θ

According to the location of displacement transducers and the plastic hinge, and the basic assumptions, the vertical absolute displacement Δ_p at the plastic hinge and the vertical absolute displacement Δ_i at the measured points in Fig. 7 can be calculated as

$$\Delta_{\mathrm{p}} = \frac{l_2 \cdot \Delta_3 - l_3 \cdot \Delta_2}{l_2 - l_3} \tag{5}$$

$$\Delta_i = \Delta_i^{'} - \frac{1}{2}(\Delta_8 + \Delta_9) \tag{6}$$

where $\Delta_i^{'}$ is the measured vertical displacement of the number i displacement transducer on the beam; Δ_i is the net displacement of the beam at the location of displacement transducer, Δ_8 and Δ_9 are the displacements at top and bottom ends of the column respectively.

Based on the above, the relative angle of the beam and the column θ can be obtained as follows.

$$\theta = \arctan\left(\frac{\Delta_{\mathrm{p}} - \delta_{\mathrm{b}}^{x_1} - \delta_{\mathrm{c}}^{x_1}}{x_1}\right) \tag{7}$$

where Δ_p is the vertical absolute displacement of the beam at the plastic hinge center, calculated from Eq. (5), δ_b^{x1} is the beam displacement caused by elastic deformation at plastic hinge center, obtained through Eq. (3), δ_c^{x1} is the beam displacement caused by the rotation of the column at plastic hinge center, calculated from Eq. (4), and x_1 is the horizontal distance between the plastic hinge center to the surface of the skin plate.

3.2 Plastic rotation angle θ_p

The beam plastic zone mostly stems from the formation of the beam plastic hinge, which could not only avoid the fracture of the beam-to-column connection but also dissipate more energy through plastic deformation to enhance seismic resistance of a frame. FEMA-267(1995) recommended a minimum plastic rotation angle should be 0.03 rad, which could be obtained as

Fig. 8 Failure mode of specimen

$$\theta_{\mathrm{p}} = \frac{\Delta_{CL}}{L_{CL}} \tag{8}$$

where Δ_{CL} is the vertical plastic displacement at the beam end (beam span center line), and L_{CL} is the distance between beam span center line and the column axis.

According to Fig. 7, the Eq. (8) could be deduced as

$$\theta_{\mathrm{p}} = \arctan\left[\frac{\frac{(L_{\mathrm{CL}} - x_1)(\Delta_1 - \Delta_{\mathrm{p}})}{(l_1 - x_1)} + \Delta_{\mathrm{p}} - \frac{\Delta_{\mathrm{p}}}{x_1} L_{\mathrm{CL}}}{L_{\mathrm{CL}}}\right] \tag{9}$$

where Δ_1 is the net displacement of the beam at the loading point and calculated by Eq. (6); Δ_p is the absolute vertical displacement at the plastic hinge center and calculated by Eq. (5).

3.3 Experimental analysis on an exterior frame joint

3.3.1 Test program

H-shaped Q235 steel column with a section of HW 300×300×10×15 (height: 3,000 mm) and H-shaped Q235 steel beams with a section of HN 350×175×7×11 (span: 1,500 mm) was used; the steel plates, too, were made of Q235 steel with a nominal yield strength of 235 MPa. The beam was connected to the skin plate using the welded-flange-bolted-web connection, a typical connection currently used in China. The test setup was shown in Fig. 6. More details of the tested specimen could be found in Lu *et al*. (2016a).

3.3.2 Test results

During the loading test, the load and displacement at the beam end increased linearly until the applied loads reached 200 kN. Then local buckling appeared on the beam flanges and web during the following loading. The load reached the maximum of 216 kN at the beam end displacement of 73 mm, then a significant drop in resistance or stiffness was observed. When the displacement was 173 mm, the load decreased to 168 kN, which was lower than 85% of the maximum load, thus the tests were halted.

Fig. 8 shows the failure mode of the proposed weak-axis connection after testing. As seen in Fig. 8, obvious yielding was observed in the beam bottom flange, indicating that the plastic hinge formed at the beam end, and the plastic hinge center was about 250 mm away from the surface of the skin plate, while the column and panel zones basically kept straight, and no damage was observed at the beam flange groove welds. It can be concluded that the proposed weak-axis connection is in accordance with the characteristics of ‘strong joint and weak member’, and ‘strong panel zone’.

Table 1 Steel material properties used in ABQUAS

Steel profiles	Thickness (mm)	Young’s modulus (MPa)	True plastic strain	True stress (MPa)
Column flange	15	2.02×10^5	0.0	285
			0.2	525
			0.4	553
			0.6	567
Skin plate	16		0.8	580
			1.0	592
Beam flange	11	2.04×10^5	0.0	307
			0.2	534
			0.4	572
			0.6	600
Column web	10		0.8	619
			1.0	635
Beam wed	7	2.06×10^5	0.0	332
			0.2	553
			0.4	607
			0.6	647
			0.8	670
			1.0	690

3.3.3 Stress distribution

The panel zone and skin plate are the key members in the proposed weak-axis connection and were instrumented extensively with tri-axis strain gauges in order to ascertain the strain profile in the proposed weak-axis connection details. Based on the measurement of strain gage rosettes under the peak load and the obtained material property, the values and directions of stresses in the column panel zone and skin plate, are depicted in Fig. 9. It is observed from this figure that:

(1) In general, the stress of measured points distributes along the diagonal direction of the panel zone, with tension along one diagonal line, and compression along the other diagonal line. Further, these stresses are significantly smaller than the corresponding yielding stress, illustrating that only tiny elastic shear deformation occurs in the panel zone, thus it can be concluded that the proposed weak-axis connection has the characteristics of ‘strong panel zone’. Relatively, larger stresses appear on the corners of panel zone, which can be attributed to the fact that the larger tensile and compressive forces of beam flange have impacted greatly to the local stresses of panel zone.

(2) The stresses of the skin plate are larger where the skin plate connected to beam flanges and web, and some stresses are close to steel material yield stress. The stresses in four corners of the skin plate, which are measured 150 mm away from the upper and lower beam flange, are relatively small and in the elastic state, indicating that the height of skin plate, which is 200 mm away from the top and bottom beam flange, may be too large, thus the height could be reduced appropriately.

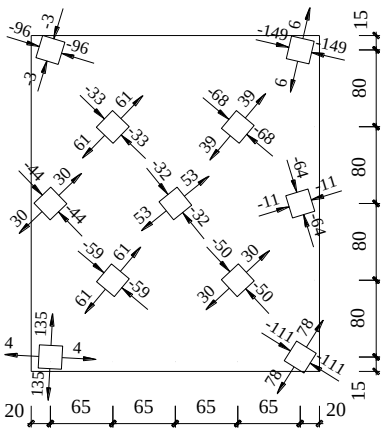

(a) Panel zone

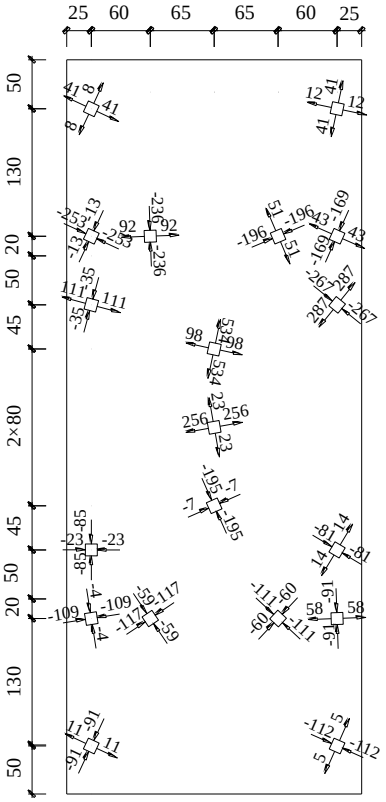

(b) Skin plate

Fig. 9* Stress distribution of panel zone and skin plate of the exterior joint

*The arrow is the direction of the principal stress and the number is the stress value in MPa

3.4 Numerical analysis on an exterior frame joint

In addition to the experimental investigation, the development and validation of an analytical model for the assessment of weak-axis exterior frame joint are also conducted. The ABAQUS software was selected for use in the numerical simulations of this study. Eight-node solid nonconforming elements C3D8I were used to reduce the number of grid units and shorten the calculation time. The plasticity model was based on the von Mises yielding criteria and the associated flow rule. The measured tensile properties of the steel profiles have been given in Lu *et al.* (2016a). Notably, the true stress and true plastic strain were adopted in the numerical analysis, as shown in Table 1.

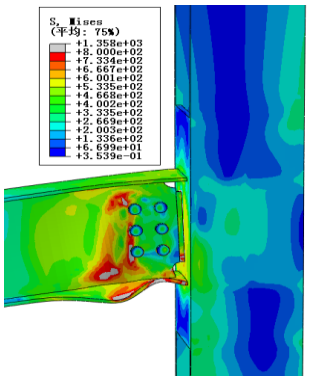

Fig. 10 Failure mode under monotonic loading

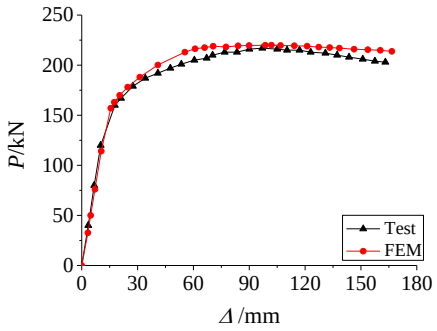

Fig. 11 Beam end load versus displacement relationships of test and FEM

The failure mode of the weak-axis exterior frame joint in numerical analysis is displayed in Fig. 10. Comparing the deformation configuration of the test and FEM in Figs. 8 and 10, the predicted buckled shape of numerical result demonstrated a good correlation with the test. Under the monotonic loading at the beam end, beam bottom flange and web experienced substantial local buckling deformations with the panel zone mainly being in the elastic state. The load-displacement relationships of the loading point at the beam end from the test and FEM are shown in Fig. 11. The initial stiffness of FEM and test matched very well and the curves showed the same trend at the plastic stage. The load that the analytical model could reach was slightly higher than that of the test, and the maximum error was 5.3%. Overall, a good agreement is obtained when compared between the experimental and numerical results.

To gain more insight into the structural behavior of the weak-axis exterior frame joint, the reference model was then investigated under cyclic loading at the beam end. Quasi-static cyclic loading with increasing vertical displacement amplitudes was adopted according to Chinese specification. The failure mode of the reference model under cyclic loading is shown in Fig. 12, and the Mises equivalent stress distribution of the skin plate is also displayed.

Under cyclic loading, the plastic hinge formed much closer to the skin plate than that of the monotonic loading, indicating that the beam flange welds were more vulnerable to brittle fracture, especially the beam bottom flange, and

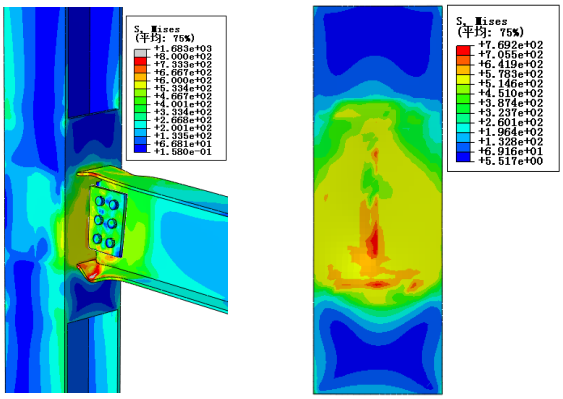

(a) Failure mode (b) Mises stress of skin plate

Fig. 12 Failure mode under cyclic loading

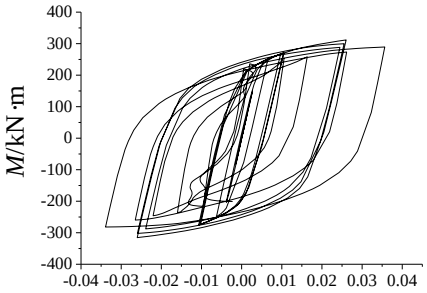

(a) M-θ curve

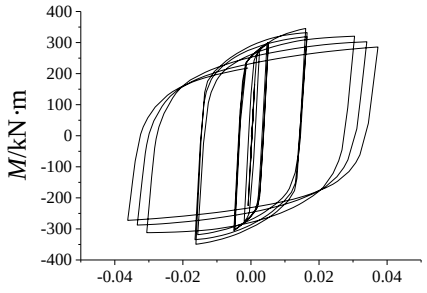

(b) M-θ_p curve

Fig. 13 Hysteretic loops of the connection under cyclic loading at the beam end

the Mises equivalent stress of the corresponding region in the skin plate was much severe.

According to the part 3.1 and 3.2, the bending moment versus rotation relationships (M-θ) and bending moment versus plastic rotation relationships (M-θ_p) curves under cyclic loading are shown in Fig. 13. If the loss of stiffness and strength at large inelastic deformation is not significant, the connection can be conceived as tough and stable. It is observed from Fig. 13 that the weak-axis exterior frame connection under cyclic loading at the beam end showed stable hysteresis performance and good deformation capacity. The maximum plastic rotation angle could reach was much larger than 0.03 rad, the requirement of FEMA-267 (1995), indicating that the proposed weak-axis connection has good plastic rotation capacity and energy dissipation capacity.

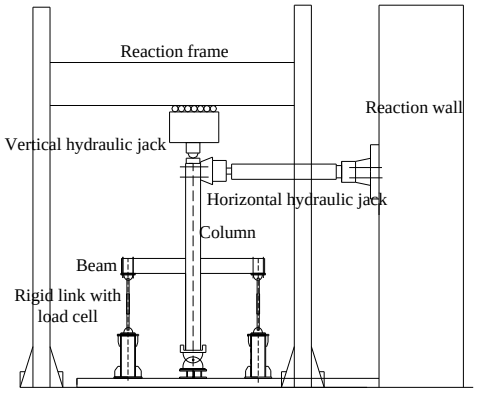

(a) Testing apparatus diagram

(b) Specimen installation

Fig. 14 Test setup of cyclic loading

4. Experimental investigation on an interior frame joint under cyclic loading

The majority of previous tests reported were about exterior frame joints with less attention being paid to interior frame joints, the most commonly used in actual engineering steel frames. In order to consider this issue and for a more in-depth study of the structural behavior of this type of weak-axis connection, a double-sided substructure subjected to horizontal cyclic loading was carried out. The test setup was designed to reproduce the boundary conditions of a beam-to-column connection substructure in a moment-resisting frame under lateral loads, as shown in Fig. 14. The specimen was assembled from two 1500 mm long HN 350×175×7×11 beams and one 4380 mm height HW 350×350×12×19 column to form the cruciform arrangement, and all steel profiles were fabricated using Q235 with a nominal yield strength of 235 MPa. The beams are connected to the skin plates using the welded-flange-bolted-web connection, similar to that of the specimen in monotonic loading test. In this test program, the P-delta effect of columns is considered so as to better simulate the real situation of structural loading with a vertical hydraulic jack used to apply a constant force of 300 kN on the top of the column firstly. Then a horizontal hydraulic actuator placed at the top of the column was used to apply horizontal cyclic loading as columns drift laterally under seismic loads in real steel frames. The horizontal loading begins with three cycles each of 10, 20, 30, and 40 mm displacement, sequentially, followed by three cycles each of successive increasing displacement (i.e., 60, 80, 100, 120, 140, 160 mm…) until failure. For brevity, only the most significant results of the test specimen are commented upon. Much

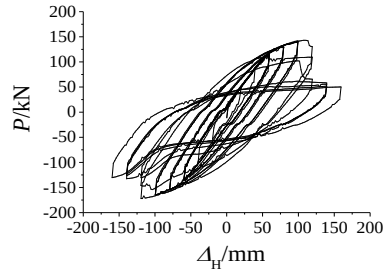

(a) Load-displacement relationships

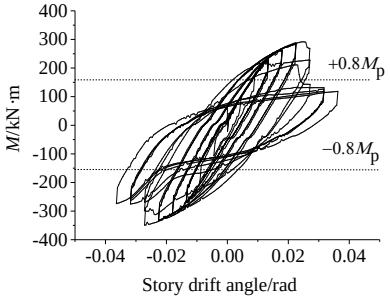

(b) Moment-story drift angle relationships

Fig. 15 Hysteretic loops of the proposed connection under cyclic loading

additional information on the tensile test results was already presented by Lu *et al*. (2017) in the companion paper.

4.1 Test results

The hysteretic loops of the column top load P versus the controlled horizontal displacement Δ_H and moment versus story drift angle are plotted in Fig. 15. The P-Δ_H hysteresis loops were stable and repetitive before the horizontal displacement reaching 100 mm, and minor local buckling of beam bottom flange could be noticed in the cycles of 100 mm. Then the weld between the diaphragm and the skin plate cracked (Fig. 16(a)) with a metallic grating noise, leading to a drastic drop of bearing capacity (Figs. 15(a)-(b)). And a crack developed in the left beam bottom flange and right beam bottom flange welds during the following cycles, resulting in the tearing of the skin plate (Fig. 16(b)). Photographs of the specimen during the test are shown in Fig. 16. The beam-to-column connections for special moment frames shall be capable of accommodating a story drift angle of at least 0.04 rad while the measured flexural resistance of the connection at the face of column shall equal at least 0.80 M_p of the beam (ANSI/AISC 341-10 2010), where the M_p is the nominal plastic flexural strength. As seen from Fig. 15(b), only the negative bending capacity met that requirement, indicating that the proposed connection could meet the requirement only under good workmanship and welding quality. It can be concluded that there was much difference between column top horizontal cyclic loading test and beam end monotonic loading test, the fracture of weld between the diaphragm and the skin plate under cyclic loading prevented the development of beam flanges yielding and buckling, thus good workmanship and welding quality are first required to provide a reliable welded connection.

4.2 Energy dissipation capacity

One of the important considerations in the evaluation of the seismic performance of a beam-to-column moment connection is its energy dissipation capacity, and it could be reflected through the area of load-displacement hysteretic loops. The energy dissipation coefficient E could be obtained as the ratio of the sum of the area of S_{ABC} and S_{CDA} to the sum of the area of S_{OBE} and S_{ODF}, as shown in Fig. 17(a). The development of energy dissipation coefficient E at each displacement amplitude is displayed in Fig. 17(b). As is observed from this figure that the energy dissipation capacity improved gradually with the increase of loading amplitudes, owing to the stable and full hysteretic loops of the specimen. The maximum energy dissipation coefficient E was about 1.7, and the corresponding equivalent viscous damping coefficient, defined as the energy dissipation coefficient E divided by 2π, was much greater than 0.2, which shows that the proposed weak-axis connection has a good energy dissipation capacity.

4.3 Stiffness degradation and bearing capacity degradation

Stiffness degradation coefficient K_i and bearing capacity degradation coefficient λ_i versus column top displacement relationships of the specimen under cyclic loading are presented in Figs. 18 and 19 respectively. The Stiffness degradation coefficient K_i and bearing capacity degradation coefficient λ_i can be calculated as

$$K_i = \frac{|+F_i| + |-F_i|}{|+X_i| + |-X_i|} \tag{10}$$

(a) Weld cracking

(b) Buckling and weld cracking and tearing of skin plate

(c) Ultimate failure mode

Fig. 16 Failure patterns

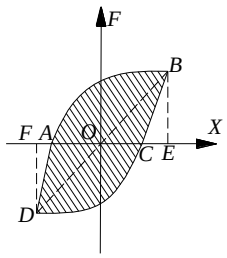

(a) Calculation method of E

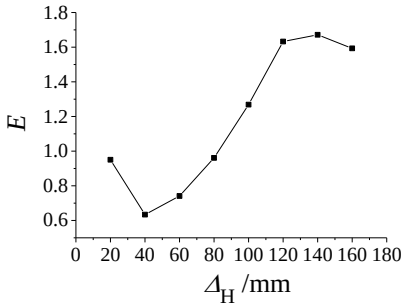

(b) Development of E

Fig. 17 Energy dissipation capacity

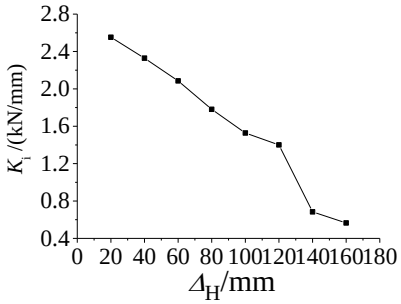

Fig. 18 Stiffness degradation curve

$$\lambda_i = \frac{F_j^i}{F_j^{i-1}} \tag{11}$$

where $+F_i$ and $-F_i$ are the positive and negative peak load in the first cycle of the i-th amplitude of the load-displacement hysteresis curves; $+X_i$ and $-X_i$ are the displacements in the first cycle of the i-th amplitude of the load-displacement hysteresis curves; F_j^i is the i-th cycle peak load at the j-th load step; F_j^{i-1} is the i-1-th cycle peak load at the j-th load step.

As evidenced from Fig. 18, the loading history was a process in which the stiffness of the substructure was declining gradually upon further loading, and the degradation slope was basically consistent and soft at the early stage, indicating that the loss of the stiffness was not significant. The fracture of the weld between the diaphragm and the skin plate caused a sharp decrease of the stiffness at the displacement amplitude of 120 mm. Fig. 19 shows the bearing capacity curves, and an asymmetric behavior was observed with greater bearing capacity under positive loading amplitude. At the early stage, the bearing capacity did not reduce the subsequent cycles of the same amplitude. The bearing capacity degradation coefficient appeared a drastic drop in the amplitude of 120 mm when a sudden

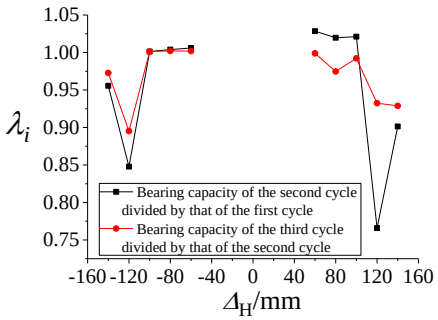

Fig. 19 Bearing capacity degradation curve

crack of the diaphragm weld occurred in the second cycle and developed in the three cycle of this amplitude. Overall, the stiffness and bearing capacity degradation of the proposed weak-axis connection under cyclic loading was not significant during the premature loading, and the break of welds would cause an unstable hysteretic response in the subsequent cycles of loading. As mentioned in the tests results, good workmanship and sound welding quality are primarily required to provide a reliable welded connection.

4.4 Stress distribution

4.4.1 Stress distribution in the panel zone and skin plate

The main aim of the strain measurement was to record the stress distribution of the panel zone, skin plate, as well as beam flanges and webs of the proposed weak-axis interior frame joint under cyclic loading. Close examination of stress readings and directions of the left panel zone and skin plate under the maximum load depicted in Fig. 20 reveals that the stress distribution was similar to that of the exterior frame joint in monotonic loading test. It is noteworthy that the values of the stress in the panel zone and skin plate of the connection under cyclic loading are much larger than that of the monotonic loading, especially in the regions of the skin plate connected to the beam flanges, where high stress led to the tearing of the skin plate after the crack of beam flange welds occurred.

4.4.2 Stress distribution in the steel beam flange

In particular, seven uniaxial strain gauges were placed along the width of beam flanges near the groove welds so that the stress state of the groove weld could be investigated in detail. Fig. 21 shows the stress distributions along the width of beam flange at the welds, and the abscissa is the obtained stress normalized by the measured material yield stress. It can be seen from Fig. 21 that the stress distributions of the top and bottom beam flange are basically identical and the stress distributions are more regular in the initial loading period. Upon further loading step, yielding of the beam flanges was detected initially near the flange groove welds, and stress concentration appeared in this location at the following cycles. This observation clearly demonstrates that the beam flange close to the beam-to-column connection develops a high local stress concentration, especially at both edges of beam flanges with the stress in excess of 10 times of the measured

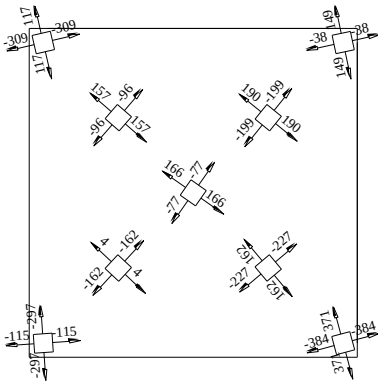

(a) Panel zone

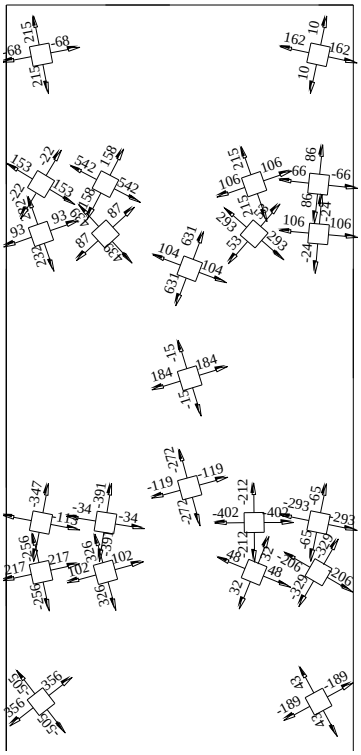

(b) Skin plate

Fig. 20* Stress distribution of panel zone and skin plate of the interior joint

*The arrow is the direction of the principal stress and the number is the stress value in MPa

yield stress. That's why the flange weld fractured initially from the edges of beam flanges during the test. Hence, it is necessary to take some technical methods to ensure the construction quality of the beam flange groove weld, such as using a backing plate and removing it after the cooling of the weld metal deposition, and then the edges of the groove weld should be ground smooth to avoid notches.

5. The influences of the proposed weak-axis connection on the steel frame

In this section, the influences of the proposed weak-axis connection on the steel frame were discussed from three aspects.

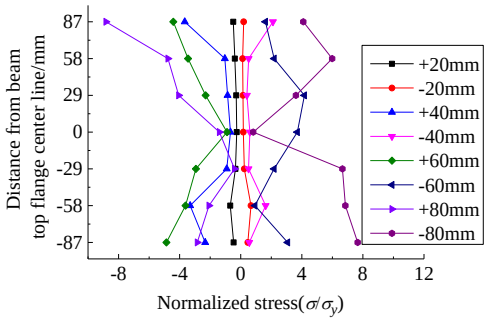

(a) Left beam top flange

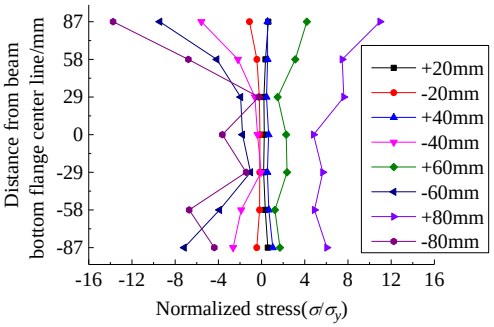

(b) Left beam bottom flange

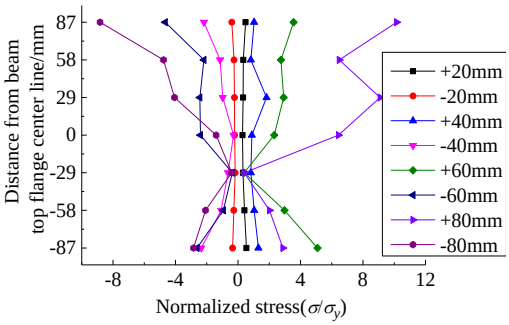

(c) Right beam top flange

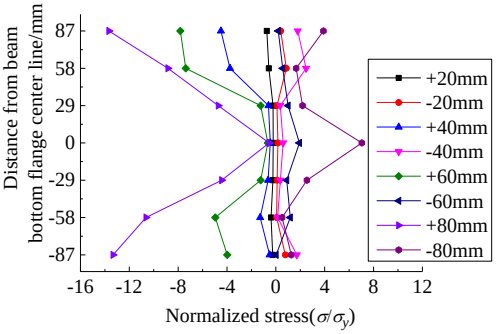

(d) Right beam bottom flange

Fig. 21 Stress distribution of beam flanges

5.1 Simplify design calculation process

Frame story drift is an important controlling index to evaluate the seismic performance of a steel moment frame. Generally, shear deformation of the panel zone must be included in the frame story drift calculation when the I-section columns were adopted in a steel frame. However, the design process is complicated and tedious, and sometimes the column section has to enlarge owing to the contribution of shear deformation of the panel zone.

Table 2 Member sections and analysis results

Item	Box-shaped column scheme	I-section column scheme
Column	H400×400×12×12	H 400×400×10×18
Beam GL-1	H 400×250×10×18	H 400×250×10×18
Beam GL-2	H 400×200×8×12	H 400×200×8×12
Slab thickness/mm	120	120
High-strength bolt	4× S10.9	4× S10.9
Skin plate	-	-850x364x16
Transverse stiffener	-376×376×18	-364×179×18
Story drift angle(X)	1/450	1/402
Story drift angle(Y)	1/382	1/390
Fundamental period	1.573S	1.724S
Axial compression ratio of column	0.57	0.62
Steel consumption of total columns/Ton	63.16	61.19

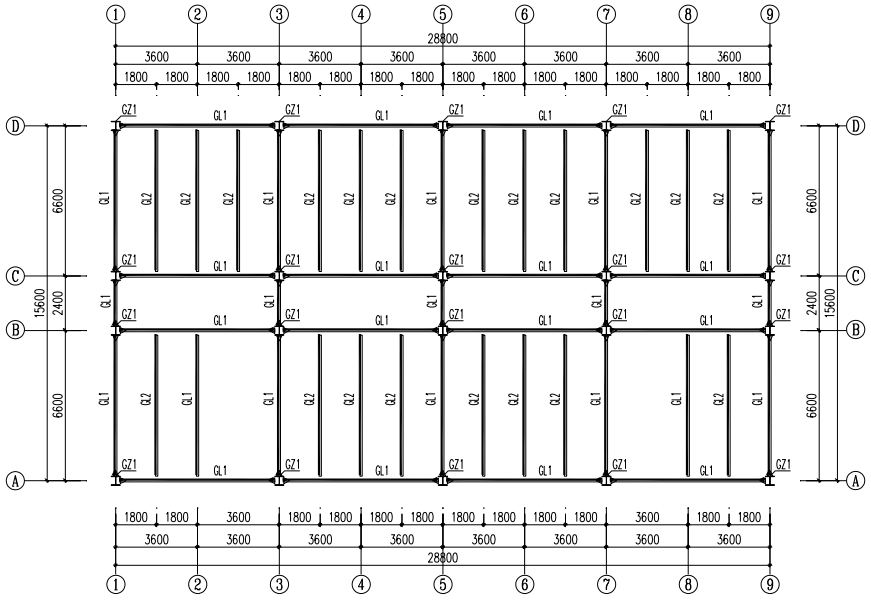

Fig. 22 Structural plane arrangement chart

An experimental study conducted on a weak-axis frame and a strong-axis frame with the proposed connection and already presented by Lu *et al*. (2016b) in another companion paper revealed that the contribution of shear deformation of the panel zone in the proposed system was only 0.7% of total story drift in strong-axis frame and 0.3% of total story drift in weak-axis frame, illustrating that the contribution of shear deformation of the panel zone in the proposed system could be neglected during the first stage of seismic design. On the one hand, this confirms that the proposed connection system can simplify the design calculation progress when I-section column is adopted in frame structural design, on the other hand, it means that the frame with proposed weak-axis connection has larger lateral stiffness and bearing capacity than the frame with the traditional weak-axis connection, and also means low construction cost.

5.2 Low construction cost in multi-story steel frames

That the box-section column is suggested when the column and beam are in rigid connection with each other in two mutually perpendicular directions were specified in China, which may increase the construction cost in some cases apparently, and I-section column is frequently used in most cases due to its economy and acceptable mechanical characteristics. This section compares the construction cost and some critical technical indexes when the proposed connection system and box-section column was adopted in a steel frame engineering project respectively. The following analysis was displayed as a part of technical supporting documents.

5.2.1 Background of the compared engineering project

Fig. 22 shows the structural plane arrangement chart of a practice project for a steel frame office building, which had been built in Xi'an city, Shaanxi Provence, China, with a total of 6-story and 3.6 m storey-height. The seismic fortification intensity is 8 degrees, and the live load is 2.0 kPa.

5.2.2 Analysis results comparison

SATWE program of 2015 version PKPM design

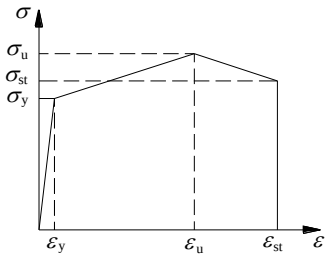

Fig. 23 Stress-strain relationships

Table 3 Material properties used in ABAQUS

Member	σ_y/Mpa	ε_y	σ_u /Mpa	ε_u	σ_{st}/Mpa	ε_{st}
Steel	235	0.00115	415	0.15	340	0.21
Bolt	940	0.00456	1130	0.1	960	0.13

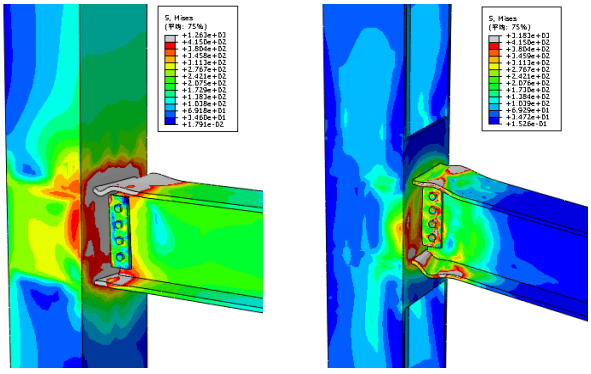

(a) Box-section column connection (b) Proposed weak-axis connection

Fig. 24 Failure mode of two connections

software was used to analyze 3-D overall structure in order to ensure that the structural member stress ratio and beam deflection meet the design specifications. Q235 steel was adopted for the beams and columns, with a specified minimum yield strength of 235 MPa. Table 2 tabulates the sections of structural members and analysis results of some critical technical indexes.

It can be seen from Table 2, the *Y* direction story drift would control the structural design, and the lateral stiffness of the proposed system was greater than that of the box-section column frame. Column axial compression ratio of the proposed system was slightly higher than that of the box-section column frame, indicating that the proposed system has higher material utilization rate, then leading to lower steel consumption.

5.3 Comparison of mechanical properties

The ABAQUS software was used for numerical simulations of the proposed connection and box-section column bending connection in order to compare their mechanical properties.

For the sake of generality, the tri-line model, which could consider the strain hardening and descend, was employed for the stress-strain relationships of steel and bolt materials, as shown in Fig. 23, and data details are listed in Table 3.

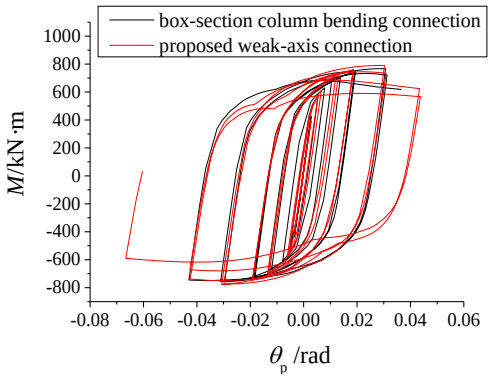

Fig. 25 Moment versus plastic rotation relationships

Fig. 24 displays the failure mode of the two connections under cyclic loading. It can be seen from Fig. 24(a) that the majority of the beam flange near the welds and the corresponding web of box-section column experienced large Mises stresses, which exceeded the ultimate strength of the steel materials, while the proposed I-section weak-axis connection showed a significant reduction of the Mises stress at the skin plate and beam end near the welds, and the beam flanges experienced evident local buckling deformations, as shown in Fig. 24(b). It can be concluded that the proposed I-section weak-axis connection could be effectively satisfied the requirements of 'strong joint and weak member'.

The bending moment versus plastic rotation relationships (M-θ_p) of the two connections is shown in Fig. 25. It is clear from the comparison of results that there was no distinct difference of moment and rotation capacity of these two connections, and the maximum positive and negative moments developed in these two connections were of comparable magnitude to each other, with the bending moment of the proposed connection slightly larger than that of the box-section column bending connection.

6. Other derivative weak-axis connections

With the connection shown in Fig. 5 as a standard prototype, by changing the beam end form, a series of derived weak-axis connections can be obtained, as displayed in Fig. 26. The first three connections, shown in Figs. 26 (a)-(c), belong to the enhanced connection; the RBS connection in Fig. 26 (d) is a classic weakened connection; the last two connections in Figs. 26 (e)-(f) belong to the semi-stiffness connection. A great deal of trial work and numerical analysis works for connections in Fig. 26 are under way, and the relative research paper will be reported successively. It is worth pointing that other successful connection forms used in strong-axis of I-section column or box-section column to H-shape beam can all be used in the proposed weak-axis connection with box-strengthened panel zone, such as the 'Sliding Hinge Joint' connection (Gregory *et al*. 2010, Ramhormozian *et al.* 2016) and external stiffener connection (Rezaifar and Younesi 2016) and T-RBS connection (Ataollahi and Banan 2016).

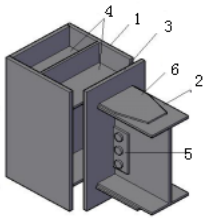

(a) Weak-axis cover-plate connection

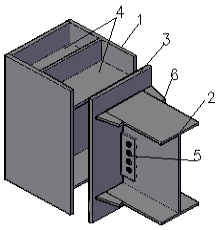

(b) Weak-axis side-plate connection

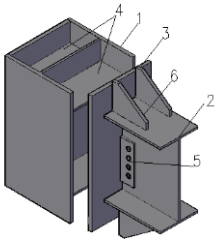

(c) Weak-axis ribs reinforced connection

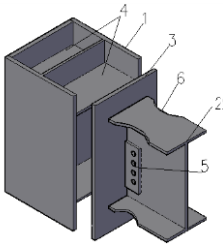

(d) Weak-axis RBS connection

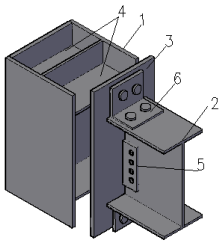

(e) Weak-axis top-and-seat angles connection

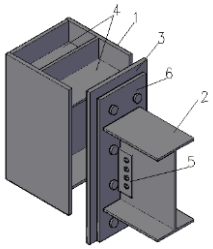

(f) Weak-axis extend end plate connection

Fig. 26 Derivative weak-axis connections

7. Conclusions

This study aims to verify the structural performance of a novel weak-axis connection with box-strengthened panel zone. Monotonic and cyclic loading experimental investigation and finite element analysis of the proposed weak-axis connection was conducted, and also a series of comparative analysis of mechanical properties and steel consumption were employed for the I-section column frame with the proposed box-strengthened panel zone and box-section column frame. On the basis of the experimental and analytical investigation, the following conclusions can be drawn.

• The proposed weak-axis connection could enable the beam to I-section column connection in weak-axis like that of strong-axis. A calculation procedure of the beam-column relative rotation and plastic rotation was proposed and described in detail, deducting the elastic deformations of beam and column.

• Under the beam end monotonic loading, no signs of fracturing were observed and the plastic hinges formed reliably in the beam section away from the beam-to-column connection; the stress of the panel zone were significantly smaller than the material yield stress, and the stresses of the skin plate region connected to beam flanges and the web are close to the material yield stress. And a good agreement is obtained when compared between the experimental and numerical results. Under the beam end cyclic loading, the plastic hinge formed much closer to the skin plate than that of the monotonic loading, but the proposed connection still has good rotation capacity and energy dissipation capacity.

• Under the column top horizontal cyclic loading, the fracture of beam flange groove weld prevented the development of beam flanges yielding and buckling, and the degradation slope of stiffness and bearing capacity was basically soft before the cracking of welds. The stresses in the panel zone and skin plate were much larger than that of monotonic loading, and the beam flange close to the beam-to-column connection developed a high local strain concentration. The fracture of welds would cause an unstable hysteretic response, thus good workmanship and welding quality are first required to provide a reliable welded connection, and it is necessary to take some technical methods to ensure the construction quality of the beam flange V groove weld.

• The proposed system could be effectively satisfied the requirements of ‘strong joint and weak-member’ and ‘strong column and weak beam’, and also has higher material utilization rate with the comparable bearing capacity to the box-section column bending connection, leading to lower steel consumption.

Acknowledgments

The authors would like to thank the Nature Science Foundation of China (NSFC) (51278061) and the Fundamental Research Funds for the Central Universities-Cultivation of Excellent Doctoral Dissertation of Chang’an University (310828175002) for the financial support.

References

ANSI/AISC 341-10 (2010), Seismic Provisions for Structural Steel Buildings, AISC, Chicago, Illinois, USA.

Ataollahi, S. and Banan, M.R. (2016), "Numerical cyclic behavior of T-RBS: A new steel moment connection", *Steel Compos. Struct.*, **21**(6), 1251-1274.

Cabrero, J.M. and Bayo, E. (2007a), "The semi-rigid behavior of three-dimensional steel beam-to-column joints subjected to proportional loading. Part I: Experimental evaluation", *J. Struct. Eng.*, **63**, 1241-1253.

Cabrero, J.M. and Bayo, E. (2007b), "The semi-rigid behavior of three- dimensional steel beam-to-column joints subjected to proportional loading. Part II: Theoretical model and validation", *J. Struct. Eng.*, **63**, 1254-1267.

FEMA-267(1995), Interim Guidelines: Evaluation, Repair, Modification and Design of Steel Moment Frames, Report No. SAC-95-02, Washington, D.C., USA.

Kim, S.D., Kim, S.S. and Ju, Y.K. (2008), "Strength evaluation of beam-column connection in the weak axis of H-shaped column", *Eng. Struct.*, **30**, 1699-1710.

Koetaka, Y., Chusilp, P., Zhang, Z., Ando, M., Suitad, K., Inoue, K. and Uno, N. (2005), "Mechanical property of beam-to-column moment connection with hysteretic dampers for column weak axis", *Eng. Struct.*, **27**(1), 109-117.

Kozlowski, A. (2016), "Component method model for predicting the moment resistance, stiffness and rotation capacity of minor axis composite seat and web site plate joints", *Steel Compos. Struct.*, **20**(3), 469-486.

Lee, E.T., Kang, M.J., Kim, S.B. and Kim, S.S. (2016), "Experimental study on structural performance of the new shaped weak-axis connection in full-scale test", *Int. J. Steel Struct.*, **16**(3), 685-696.

Lee, K., Li, R., Jung, H., Chen, L. and Oh, K. (2013), "Cyclic testing of weak-axis steel moment connections", *Steel Compos. Struct.*, **15**(5), 507-518.

Lee, K., Li, R., Jung, H., Chen, L., Oh, K. and Kim, K.S. (2014), "Cyclic testing of steel column-tree moment connections with various beam splice lengths", *Steel Compos. Struct.*, **16**(2), 221-231.

Lee, S.J. and Lu, L.W. (1989), "Cyclic tests of full-scale composite joint subassemblages", *J. Struct. Eng.*, **115**(8), 1977-1998.

Lu, L.F., Xu, Y.L. and Zheng, H. (2017), "Investigation of composite action on seismic performance of weak-axis column bending connections", *J. Constr. Steel Res.*, **129**, 286-300.

Lu, L.F., Xu, Y.L., Zhou, T.H. and Zheng, H. (2016a), "Experimental research on box strengthened joint connection for weak axis of I-section column-H-shaped beam under monotonic loading", *J. Build. Struct.*, **37**(2), 73-80.

Lu, L.F., Yuan, Y., Zhou, T.H. and Zheng, H. (2016b), "Experimental study on seismic behavior of box strengthened joint region for steel frames with I-section column", *J. Build. Struct.*, **37**(7), 64-73.

MacRae, G.A., Clifton, G.C., Mackinven, H., Mago, N., Butterworth, J. and Pampanin, S. (2010), "The sliding hinge joint moment connection", *Bul. NZ. Soc. Earthq. Eng.*, **43**(3), 202-212.

Ramhormozian, S., Clifton, G.C. and Macrae, G.A. (2016), "Recent developments on the sliding hinge joint", https://www.researchgate.net/publication/300044677.

Rezaifar, O. and Younesi, A. (2016), "Finite element study the seismic behavior of connection to replace the continuity plates in (NFT/CFT) steel columns", *Steel Compos. Struct.*, **21**(1), 73-91.

Shim, H.J., Lee, E.T., Kim S.B. and Kim, S.S. (2014), "Development and performance evaluation of weak-axis column bending connections for advanced constructability", *Int. J. Steel Struct.*, **14**(2), 369-380.

CC